PCCP

Accepted Manuscript

ROYAL SOCIETY OF CHEMISTRY

www.rsc.org/pccp

Physical Chemistry Chemical Physics
CREATED USING THE RSC LaTeX PCCP ARTICLE TEMPLATE – SEE www.rsc.org/electronicfiles FOR DETAILS
ARTICLE TYPE www. rsc.org/xxxxxx | XXXXXXXX

Fragmentation Dynamics in Dissociative Electron Attachment to CO probed by Velocity Slice Imaging

Pamir Nag and Dhananjay Nandi*

Received Xth XXXXXXXXXX 20XX, Accepted Xth XXXXXXXXX 20XX
First published on the web Xth XXXXXXXXXX 200X
DOI: 10.1039/b000000x

Complete dissociation dynamics in electron attachment to carbon monoxide (CO) have been studied using the newly developed Velocity Slice Imaging (VSI) technique. Both kinetic energy and angular distributions of O^- ions formed by dissociative electron attachment (DEA) to CO molecule have been measured for 9, 9.5, 10, 10.5, 11, 11.5 eV incident electron energies around the resonance. Detailed observations conclusively show two separate DEA reactions lead to the formation of O^- ions in the ground ^2P state along with the neutral C atoms in ground ^3P state and first excited ^1D state, respectively. Within the axial recoil approximation and involving four partial waves, our angular distribution results clearly indicate that the two reactions leading to O^- formation proceed through the specific resonant state(s). For the first process, more than one intermediate states are involved. Whereas, for the second process, only one state is involved. The observed forward-backward asymmetry is explained due to the interference between the different partial waves that are involved in the processes.

1 Introduction

Carbon monoxide (CO) is a simple heteronuclear diatomic molecule, much more chemically stable toxic gas (commonly known as poisonous gas), occurs in nature as a product of oxidation or combustion of organic materials. It is well known that CO also arises in cells and tissues as a by product of heme oxygenase activity.[1] Innumerable deaths have results from CO due to incomplete combustion of organic materials. Although it has enormous applications in various branches of science, very little attention has been taken on its significance due to the bad reputation. However, CO has become an important gas in biology and medicine,[1] shares many properties with nitric oxide (NO), an established cellular messenger. Electron collision studies also showed some similarity between these two molecules. In contrast to the toxic behavior of CO at high concentration, low concentration CO play an important role in different biological processes. CO produced in body during normal cellular metabolism and it may participate in neural signaling. It is believed that CO might have effect in regulating blood vessel tone, it has anti-inflammatory and anti-apoptotic property. CO might have medical application as well like in organ transplantation, vascular disease, cancer, lung injury, hepatitis and many more. CO also plays an important role in production of Ozone gas in upper atmosphere. CO is the second most common molecule in inter-stellar medium, can be used as a tracer of molecular cloud.[2] Extremely high velocity CO emission also has been observed in high mass prostar in the recent time.[3] The study of electron interaction with such important molecule is very scarce. In this context we performed kinematically complete measurement in low energy electron collision with such molecule.

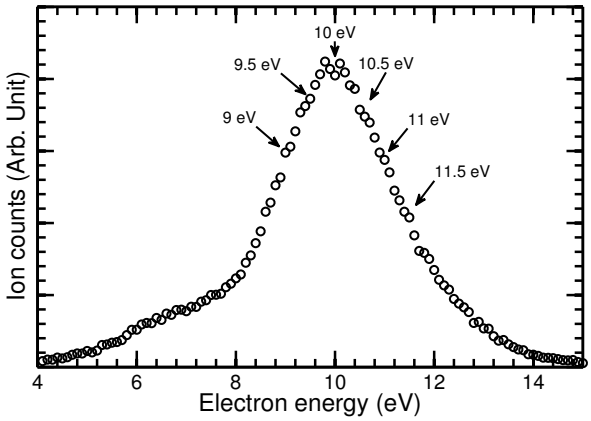

Fig. 1 Ion yield curve of O^- produced from DEA to CO. The arrows indicate the electron energies at which the images are taken.

The O^- ion formation from CO due to electron impact was first observed by Vaughan[4] back in 1931. Rapp and Briglia[5] measured the absolute cross section of negative ions and reported to observe the dissociative electron attachment (DEA) peak near 9.9 eV. Based on electron energy dependent cross sections measurements and kinetic energy distributions of O^- ions Chantry[6] identified two separate channels leading to O^- formation from CO due to DEA. The predominant process

Indian Institute of Science Education and Research, Kolkata, Mohanpur, Nadia 741246, India; E-mail: dhananjay@iiserkol.ac.in

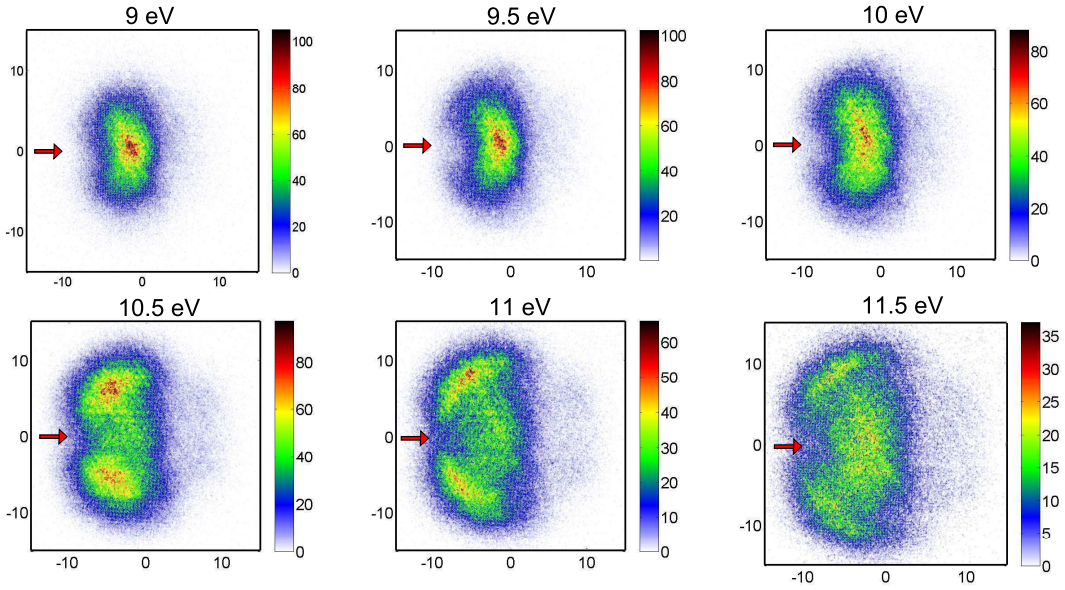

Fig. 2 Time sliced images at different incident electron energies. The incident electron beam direction is along the horizontal axis from left to right through the center of each image, the small arrows indicate the electron beam direction.

leading to O^- formation, having an energy threshold of 9.62 eV:

$$e^- + CO(^1\Sigma^+) \rightarrow CO^{-*} \rightarrow O^-(^2P) + C(^3P), \quad \text{(process I)}.$$

Another process with energy threshold 10.88 eV, proposed by Chantry is,

$$e^- + CO(^1\Sigma^+) \rightarrow CO^{-*} \rightarrow O^-(^2P) + C^*(^1D), \quad \text{(process II)}.$$

Recently, the threshold energies for the O^- production were revisited using very high energy resolution experiments[7] on DEA to CO. Denifl *et al.*[7] clearly observed two resonant peaks corresponding to the process I and II. The observed small peak (about 5%, over the neighbouring low energy peak) in their ion yield curve is due to the process II. Another channel leading to C^- formation with low cross section was observed by Stamatovic and Schulz.[8] Due to very low C^- formation cross section, the present experiment focuses only on O^- ions generated by above mentioned two processes. Almost four decades back, Hall *et al.*[9] measured both the kinetic energy and angular distributions of the O^- ions using an electron-impact spectrometer with a good precision and sensitivity. The observed kinetic energy distribution strongly supported the conclusion made by Chantry. Hall *et al.* attempted to determine the symmetries and configuration of the resonant states involved in the process by measuring the O^- angular distributions using conventional turn-table experiment. From the angular distribution data taken over a limited angular range, Hall *et al.* proposed the intermediate state to be a Π state for both the processes and ruled out the possibility of a $\Sigma \rightarrow \Sigma$ transition based on Dunn's selection rule.[10] Notice that their angular distribution data showed some distribution in the forward direction (in the range of 30° to 90°), however, they could not conclude due to lack of data in forward direction. Morgan *et al.*[11] recently computed the potential energy curve of the neutral CO molecule and the resonance states using R-matrix formalism. In the recent time, velocity map imaging (VMI)[12,13] with time slicing[14–16] technique have been developed and implemented in DEA studies,[17–21] from diatomic to polyatomic molecules. Velocity slice imaging (VSI) in its various forms have helped to study both the kinetic energy and angular distribution simultaneously with higher accuracy and sensitivity. In contrast to the conventional turn-table experiment, VSI technique neither require to rotate the electron gun nor the spectrometer and is superior and less erroneous. Very recently Tian *et al.*[22] applied such technique to study the angular distribution of O^- ions from CO due to DEA and proposed the presence of coherent interference between the different states that are involved for process I, but have not discussed the process II. They fitted the angular distribution data for 10 eV incident electron energy with a two state combination of Σ and Π intermediate states with interference. They also reported to observe near zero eV O^- ions for 10.6 eV incident electron energy, but very poor intensity and have not provided angular distribution. Very recently, we developed a modified velocity slice imaging spectrometer to study the low and intermediate energy electron-molecule collision experiments. In this article, we report the kinetic energy distribution of the O^- ions over a broad incident electron energy range of 9 eV to 11.5 eV

around the resonance and also the angular distribution of the O^- ions created by process I and II separately over the entire 2π angle. Here we report for the first time the angular distribution data over 2π angle for the process II. In contrast to Hall *et al.*, we found the intermediate state to be mainly a Σ state for both the processes. We also have observed that there is no need to include the coherent interference between different states as proposed by Tian *et al.*

2 Instrumentation

Negative ions are formed due to low energy electron capture and subsequent dissociation. The measurements are performed under high vacuum condition at the base pressure below $\sim 10^{-9}$ mbar. A magnetically well collimated pulsed electron beam of 200 ns duration, 10 kHz repetition rate and with controlled energy is passed through the interaction region where it interacts with an effusive molecular beam produced by a capillary tube. The molecular beam is directed towards the detector and along the axis of the spectrometer. We have used a custom build electron gun consisting of thermally heated filament with typical resolution of 0.8 eV. The magnetic field used to collimate the electron beam is about 40 Gauss. A pair of magnetic coil (Helmholtz type) is mounted outside the vacuum chamber to produce the uniform magnetic field at the interaction region. After it has passed, a negative pulsed extraction field is applied and the negative ions are extracted from the source region into the VMI spectrometer. The extraction pulse duration used in the present experiment is 4 μs and is applied 100 ns after the electron gun pulse. The delayed extraction provide appropriate time spread for better time sliced image. The VMI spectrometer is like a three field time-of-flight spectrometer[17] which focuses ions starting from a finite volume onto a two-dimensional position sensitive detector such that ions with a given velocity are mapped to a point on the detector irrespective of their spatial location in the source region. The two-dimensional position sensitive detector consists of three micro channel plates (MCPs) in Z-stack configuration and a three layers delay line hexanode.[23] The time-of-flight (ToF) of the detected ions is determined from the back MCP signal whereas the x and y positions of each detected ions are calculated from the three anode layers[23] placed behind the MCPs. The x and y position along with ToF of each detected particles are acquired and stored in a list-mode format (LMF) using the CoboldPC software from RoentDek. The central slice through the 'Newton Sphere' contains the full angular and translational energy information. The central sliced image is obtained by selecting appropriate time window during the off-line analysis from the stored LMF file using the same CoboldPC software. Such time sliced image corresponds to the ions ejected in the plane parallel to the detector containing the electron beam axis.

The typical full width at half maximum (FWHM) of the ToF of the O^- ions produced in this energy range is about 250 ns. We have taken a 50 ns time sliced image from the central part of the entire Newton Sphere. The complete information about the kinetic energy released and angular distribution of the negative ions can be obtained from this central slice. For incident electron beam energy calibration we have considered the O^-/CO resonance peak (shown in Fig. 1) to be at 9.9 eV.[5] To measure the kinetic energy release (KER) of the negative ions we have calibrated our system using the energy release of O^-/O_2 at 6.5 eV.[24] We also have cross-checked the kinetic energy calibration by measuring the kinetic energy of O^- produced by electron attachment at 8.2 eV of CO_2.[25]

To obtain the ion yield curve a different set of data acquisition system has been used. For this purpose the signal from MCP only has been taken. The MCP signal is amplified through a Fast Amp and then fed to a Constant Fraction Discriminator (CFD). The output from CFD is fed to STOP of a Nuclear Instrumentation Module (NIM) standard Time-to-Amplitude Converter (TAC) and START is generated from the master pulse used in the electron gun. The output of the TAC is connected to a Multichannel Analyser (MCA, Ortec model ASPEC-927) and finally communicated with the data acquisition system installed in a dedicated computer via high-speed USB 2.0 (Universal Serial Bus) interface. A home made LabVIEW based data acquisition system has been used to get the ion yield curve. Using this software at first the ToF has been obtained, then by selecting only the channels corresponding to a particular mass, the electron energy versus the number of ions produced have been measured.

3 Results and Discussion

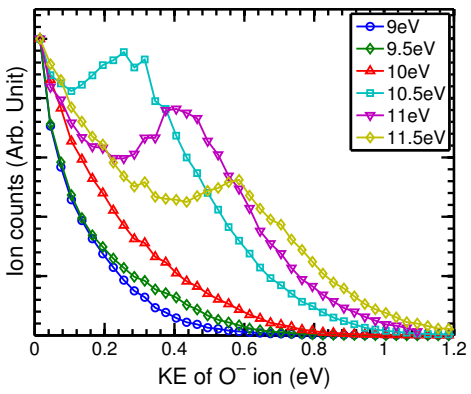

Fig. 3 The unweighted kinetic energy distribution of the O^- ions created due to interaction with different incident electron energies. The number of counts are normalized at the near zero eV value.

Fig. 1 shows the ion yield curve of O^- ions produced from CO due to dissociative electron attachment (DEA) process. Due to poor electron beam energy resolution, we are unable to separate out the two above mentioned processes from the ion yield curve only. However, as discussed in the following section we can clearly resolve the two closely lying resonances from the sliced images. The arrows in Fig. 1 indicate the energies at which the velocity slice images (VSI) are taken. The central sliced images at different incident electron energies are shown in Fig. 2. The small arrows indicate the electron beam direction. Both the kinetic energy of the O^- ion fragments and the angular distributions for a given incident electron energy can simultaneously be obtained from the corresponding time slice images. From Fig. 2, an interesting behavior has been observed in the pattern evolution of the images as the incident electron energy increases. The first image taken at 9 eV shows an oval shape with backward peaking intensity and near zero kinetic energy (KE). As the electron energy increases, upto 10 eV, the general feature in the pattern remains same with the increased shape due to the increase in KE. A similar phenomena have been observed by Nandi *et al.*[26] in the DEA studies to NO molecule in the VSI pattern evolution. Notice, the image taken at 9.5 eV is quite similar as observed by Tian *et al.* A dramatic change has been observed in the distribution while going from 10.0 to 10.5 eV. Apart from backward peak with definite KE, an additional distribution starts appearing with near zero KE and again backward peaking distribution. From the observed distributions, we can conclude that upto 10 eV the process I is involved, whereas, above 10 eV both the processes are open. Tian *et al.*[22] also reported to observe some near zero eV O^- ions for 10.6 eV electron energy. No attempt has been made by them to identify the two processes separately, kinetic energy distribution information of the O^- ions for different electron energies and angular distribution for the second process are also not reported. In the angular distribution Tian *et al.*[22] did not observed any forward peak for higher energy. Another point to be noted that the switch over energy is 10.5 eV in our case, whereas 10 eV for Tian *et al.* case. This difference could be due to different calibrations used in different experiment. Tian *et al.*[22] have not reported the resonance (ion yield) curve and we calibrated the electron energy using the reported peak energy to be 9.9 eV.[5] Furthermore, we also have crosschecked the electron energy by studying O^-/O_2 before and after the measurements taken for CO.

3.1 Kinetic energy distribution

By visual inspection of the central slices (Fig. 2) only it is clear that, the process upto 10 eV incident electron energy and above 10.5 eV are quite different. The available energy in the process is distributed among the neutral carbon atoms and the O^- ions. From energy and momentum conservation the kinetic energy (KE) available for the O^- ions can be obtained from,

$$E_R = \left(1 - \frac{m}{M}\right)[V_e - (D - A + E^*)] \quad (1)$$

where, m and M are the masses of O^- ion and neutral CO molecule respectively. V_e is the energy available to the center-of-mass system, basically the incident electron energy. D is the dissociation energy of the neutral CO molecule, A is electron affinity of O^- ion fragment and E^* is the excitation energy of the neutral C atom. Using the standard values of $m = 16$ amu, $M = 28$ amu, $D = 11.09$ eV,[27] $A = 1.47$ eV[28] and E^* for $C(^3P)$ is 0 eV and for $C(^1D)$ is 1.26 eV[29] one can get the KE of O^- fragment produced from CO due to process I and II for different incident electron energies. The calculated values are shown in the Table 1. The unweighted KE distributions of the O^- ions for different incident electron energies are shown in Fig. 3. For 9, 9.5 and 10 eV electron energies only one peak is present but for 10.5 eV and above another peak appears in the KE distribution curve. Clearly upto 10 eV only one process and from 10.5 eV two processes get involved. By comparing the measured KE of O^- ions and the computed values for the same using equation (1) (see Table 1) we can conclude that the single KE peak for 9, 9.5 and 10 eV and the higher energy peak for 10.5 eV and above incident electron energies are due to the process I, whereas, the near zero eV KE peaks for 10.5, 11 and 11.5 eV electron energies are due to process II. The slight discrepancy between the computed and measured values are due to the poor energy resolution of the electron gun, which is around 0.8 eV. Considering the 0.8 eV energy uncertainty in the calculation we found that the computed values and measured values are matching quite satisfactorily. An attempt has been made to obtain the threshold energies for both the processes using the most probable KE from the KE distributions taken at different electron energies. Fig. 4 displays the most probable kinetic energy vs incident electron energy for both the processes. Notice for process I, we considered only higher electron energy data, whereas for the process II, we have taken all three data. Linear fit to data and extrapolation to the x-axis provides the energy threshold for the process. Within our confidence level, we observed the

Table 1 Kinetic energy of O^- ions from thermochemical consideration for both the processes I and II

	KE for Process I (eV)	KE for Process II (eV)
9 eV	-0.2	-
9.5 eV	-0.05	-
10 eV	0.163	-
10.5 eV	0.377	-0.164
11 eV	0.591	0.049
11.5 eV	0.806	0.264

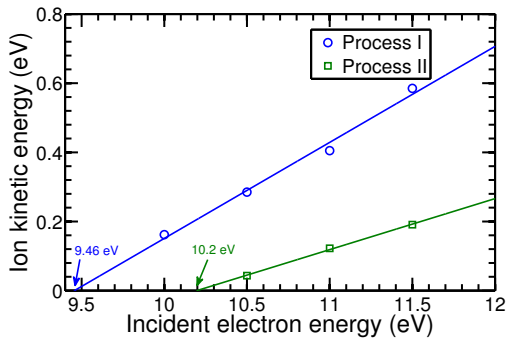

Fig. 4 The most probable kinetic energy versus incident electron energy curve of O^- ions created due to processes I and II. Liner fit for both data are also shown. The fitted line intersect the x-axis at 9.46 eV and 10.2 eV for process I and II, respectively.

threshold energies to be 9.46 eV for the process I, and 10.2 eV for the process II, respectively. Within the experimental error these values match well with the previously reported values of 9.62 and 10.88 eV for process I and II respectively.[6]

3.2 Angular distribution

To know about the symmetry of the intermediate state(s), the angular distribution of the O^- ions created due to process I and II have been studied separately. For 9, 9.5 and 10 eV incident electron energies ions created with kinetic energy between 0 to 0.65 eV are considered (due to process I) in angular distribution measurement and for 10.5, 11 and 11.5 eV electron energies ions with kinetic energy between 0.1 to 0.65 eV, 0.25 to 0.65 eV and 0.4 to 1.0 eV respectively considered to be created due to process I. Whereas, O^- ions with KE between 0 to 0.1 eV, 0 to 0.25 eV and 0 to 0.40 eV for incident electron energies of 10.5, 11 and 11.5 eV respectively, are considered to be created due to the process II during angular distribution measurement. The angular distribution data are fitted using different states and four partial waves for each state. According to O'Mallay and Taylor[30] the angular distribution of the ions have the general form for diatomic molecule as

$$I(k,\theta,\phi) \sim \left| \sum_{L=|\mu|}^{\infty} a_{L,|\mu|}(k) Y_{L,\mu}(\theta,\phi) \right|^2 \qquad (2)$$

due to the involvement of each resonant state. Where, k is the incident electron momentum, $a_{L,|\mu|}$ are energy dependent expansion coefficients and $Y_{L,\mu}$ are the spherical harmonics. $\mu = |\Lambda_f - \Lambda_i|$, where Λ_i and Λ_f are the projection of the electronic axial orbital momentum along the molecular axis for the initial and final molecular states, respectively. For heteronuclear diatomic molecules like the present case, $L \geq |\mu|$, whereas, for homonuclear diatomic molecules L values are also restricted to even or odd depending on whether the initial and final states have same or opposite parity. Here, the spin conservation follows since the extra electron carries $\pm\frac{1}{2}$ spin. We have fitted the measured angular distribution using the equation

$$I(\theta) \sim \sum_{|\mu|} \left| \sum_{j=|\mu|} a_j Y_{j,\mu} e^{i\delta_j} \right|^2 \qquad (3)$$

The summation over μ take care of the involvement of the different states in the process. The ground state of neutral CO molecule is $^1\Sigma^+$ ($\Lambda_i = 0$). So, in the present case, μ=0, 1, 2 and 3 represent a transition to Σ, Π, Δ and Φ states respectively, a_j's are the relative weighting factor of the different partial waves, δ_j's denote the phase differences of the each partial waves with respect to the lowest order partial wave responsible for that particular transition. The potential energy curve calculated by Morgan *et al.*[11] shows in Franck-Condon transition region near the resonance energy Σ, Π, Δ and Φ are present. So, the temporary CO^- ion may be formed in any of these states.

Fig. 5 (a) represents the measured angular distribution data obtained from different incident electron energies for the process I. Fig. 5 (b) and (c) shows the angular distribution data for 9.5 and 11 eV electron energies respectively along with the fitted curves for $\Sigma \rightarrow \Sigma$ and $\Sigma \rightarrow \Pi$ single state transitions and to a $\Sigma \rightarrow \Sigma, \Pi$ two states transition models. For process I, the best fit is obtained a $\Sigma \rightarrow \Sigma, \Pi$ two state transition model, of the form $|\sum_{j=0}^{3} a_j e^{i\alpha_j} Y_{j,0}|^2 + |\sum_{k=1}^{4} b_k e^{i\beta_k} Y_{k,1}|^2$. The fitted parameters are shown in Tables 2 and 3, respectively. However, transition to a Δ state can also roughly describe the angular distribution for 10.5 eV and above. But, overestimates the intensities around 30° and 330° and largely underestimates around 180°. A Δ state, theoretically predicted by Morgan and Tennyson,[11] might also gets involved but, contribution is vanishingly small. By fitting the data for transition to different states, we found for the process I, the Σ state is always present, the contribution of Π state increases with increasing incident electron energies and before 10.5 eV the contribution of Π state is vanishingly small. Around 10 eV a $^3\Sigma^+$ state of CO was suggested by Sanche and Schulz.[31] Comer and Read[32] also discussed the presence of this state as a Feshbach resonance. Hall *et al.* argued that $^3\Sigma^+$ state having large permanent negative dipole moment (value -1.05 D)[33] will produce O^- ions having peak in backward direction only. While Π state, having large positive dipole moment, will contribute in forward peaking. The angular distributions show that upto 10 eV incident electron energies only two large backward peaks are present but for 10.5 eV and above electron energies two small forward peaks near 30° and 330° appear. These forward peaks are due to the small contribution from a resonant Π state. According to Dunn's selection rule[10] for heteronu-

clear diatomic molecule, along 180° a $\Sigma \rightarrow \Sigma$ transition is allowed but $\Sigma \rightarrow \Pi$ is forbidden. The angular distributions data show that the normalized ion counts along 180° decrease with the incident electron energies. Hall *et al.*[9] suggested the intermediate state for process I to be a Π state and also concluded that Σ state is absent from their angular distributions data taken over a limited angular range. They extrapolated the data presuming it to be zero at 180° and using Dunn's selection rule came to such conclusion. But our angular distributions data taken over entire 360° angle simultaneously show large forward-backward asymmetry. Such large forward-backward asymmetry have been reported recently by Tian *et al.*[22]. But there are some striking differences between present angular distribution data and Tian *et al.*'s results. For 10 eV incident electron energy they got some ions along 180° but for 10.6 eV energy zero counts along 180° but in our angular distribution data for process I, the counts along 180° decreases with increasing electron energy but it never goes to zero. For 10.6 eV they have not noticed any forward peak but, from 10.5 eV we got two small forward lobes around 30° and 330°. From the fit parameters, effect of dipole moment and considering Dunn's selection rule, we conclude that, in process I the intermediate state is mainly Σ state with a minor contribution from Π state that increases with increase in incident electron energies.

Fig. 6 (a) shows the angular distribution of O^- ions created due to process II, for 10.5, 11 and 11.5 eV incident electron energies. The angular distributions of O^- ions created due to process II are also fitted with different models. Fig. 6 (b) shows the angular distribution data for 11 eV electron energy and the fitted curves for $\Sigma \rightarrow \Sigma$ and $\Sigma \rightarrow \Pi$ single state transitions and to a $\Sigma \rightarrow \Sigma, \Pi$ two states transition models. We found the best fit is a $\Sigma \rightarrow \Sigma$ transition, using the equation $|\sum_{j=0}^{3} a_j e^{i\alpha_j} Y_{j,0}|^2$. Fig. 6 (b) shows the angular distribution for 11.5 eV incident electron energy with the fit. The fit parameters are listed in Table 4. Hall *et al.*[9] proposed the intermediate state for the process II also to be a Π state and Σ state is absent from their angular distribution data taken over a limited range. As already discussed for process I, Hall *et al.* presume the ions counts to be zero at 180° for process II and came to such conclusion. We found some O^- ions along 0° and very large number of ions along 180°. According to Dunn's selection rule[10] only a intermediate Σ state will produce ions along 0° and 180°. So from the data fit and Dunn's selection rule we conclude the intermediate state in process II is a Σ state. Fitting with Δ and Φ show that they are not present at all in the process II. A minor contribution from a resonant Π state might be present.

In a recent study, Tian *et al.*[22] reported the angular distributions of O^- ions from CO due to DEA for two electron energies, no kinetic energy distributions were reported. In Fig. 2 of Tian *et al.*[22] showed that the central slice images taken at 9.5 and 10 eV give completely different behavior. We also have observed the similar effect while going from 10 to 10.5 eV. We have studied the ion yield curve (Fig. 1) and consider the peak energy to be 9.9 eV.[5] We have performed the energy calibration by checking before and after taking each set of VSI. Above mentioned energy difference could be due to different energy calibration used in different experiments. Tian *et al.* considered interference between different states to fit the angular distributions. They reported that the fitted curves by considering interference and without interference are almost same for the data at 10 eV. But, they argued for 10.6 eV incident electron energy the interference between different states not only changes the forward-backward asymmetry but also eliminates two small forward lobes around 30° and 330° predicted by the same model without interference term but are absent in their experimental data. Surprisingly, we have observed the two small forward lobes due to process I from 10.5 eV onwards electron energies. Hall *et al.*[9] discussed such interference effect if any would necessarily be weak that could result small asymmetry. The argument was with such small energies, if two states with different symmetry couples (rotationally), it would be reasonably small. Thus the interference between the states proposed by Tian *et al.* might not be correct. Strong forward-backward asymmetry have been observed in DEA to various other molecules like NO,[26] that could be explained using the interference between different partial waves of the same state as has been done in the present report. We believe that it is not require to include the interference between different states to describe the angular distributions, the interference between different partial waves of each states is sufficient to describe the forward-backward asymmetry.

4 Conclusion

In summary, we clearly identified two closely lying resonances in DEA to CO as suggested by Chantry[6] using highly differential momentum imaging experimental technique. We have measured the kinetic energy distribution of O^- ions and identified the two different processes leading to O^- formation. The angular distribution of the O^- ions created by the two processes have also been studied separately. In contrast to Hall *et al.* we found for both the processes Σ state is always present. In process I, minor energy dependent contribution from Π state also observed. We do not find any evidence to include the interference effect between different states, as proposed by Tian *et al.*[22] to describe the angular distribution data.

References

1 S. W. Ryter and L. E. Otterbein, *BioEssays*, 2004, **26**, 270–280.
2 T. Liu, Y. Wu and H. Zhang, *The Astrophysical Journal Letters*, 2013, **775**, L2.

Table 2 Fitting parameters for the angular distribution of the O^- ions taken at 9, 9.5 and 10 eV incident electron energies. These ions are created by process I. The angular distributions are fitted with Σ to Σ and Π transition.

	9 eV	9.5 eV	10 eV
Weighting ratio of different partial waves			
a_0: a_1: a_2: a_3:	1: 0.56: 0.25: 0.45:	1: 0.42: 0.13: 0.14:	1: 0.54: 1.03: 0.10:
b_1: b_2: b_3: b_4	0.72: 0.22: 0.56: 0.03	0.36: 0.16: 0.22: 0.00	2.10: 1.15: 0.32: 0.08
Phase difference (Σ)			
$\delta_{s-p}, \delta_{s-d}, \delta_{s-f}$ (rad)	3.472, 3.457, 1.486	3.068, 2.387, 0.310	3.968, 2.224, 5.036
Phase difference (Π)			
$\delta_{p-d}, \delta_{p-f}, \delta_{p-g}$ (rad)	2.403, 4.956, 4.876	5.447, 1.48, 0.803	3.885, 0.0, 5.003

Table 3 Fitting parameters for the angular distribution of ions created due to process I, for incident electron energies of 10.5, 11 and 11.5 eV. The angular distributions are fitted for a Σ to Σ, Π transition.

	10.5 eV	11 eV	11.5 eV
Weighting ratio of different partial waves			
a_0: a_1: a_2: a_3:	1: 0.65: 0.28: 0.26:	1: 0.72: 0.26: 0.26:	1: 0.99: 0.00: 0.52:
b_1: b_2: b_3: b_4	0.04: 0.19: 0.28: 0.12	0.56: 0.35: 0.51: 0.20	0.80: 0.60: 0.75: 0.06
Phase difference (Σ)			
$\delta_{s-p}, \delta_{s-d}, \delta_{s-f}$ (rad)	3.613, 2.496, 0.879	3.619, 2.523, 1.069	3.438, 2.116, 0.6172
Phase difference (Π)			
$\delta_{p-d}, \delta_{p-f}, \delta_{p-g}$ (rad)	0.009, 2.216, 0.825	2.340, 4.655, 0.042	4.037, 2.263, 0.596

Table 4 Fitting parameters for the angular distribution of O^- ions created by process II for 10.5, 11 and 11.5 eV incident electron energies. The angular distributions are fitted for a Σ to Σ transition only.

	10.5 eV	11 eV	11.5 eV
Weighting ratio of different partial waves			
a_0: a_1: a_2: a_3	1: 0.56: 0.17: 0.04	1: 0.70: 0.26: 0.09	1: 0.32: 0.15: 0.09
Phase difference			
$\delta_{s-p}, \delta_{s-d}, \delta_{s-f}$ (rad)	2.033, 3.231, 4.49	4.170, 2.922, 1.597	3.881, 2.105, 0.975

3 K. Qiu, F. Wyrowski, K. M. Menten, R. Gsten, S. Leurini and C. Leinz, *The Astrophysical Journal Letters*, 2011, **743**, L25.
4 A. L. Vaughan, *Phys. Rev.*, 1931, **38**, 1687–1695.
5 D. Rapp and D. D. Briglia, *The Journal of Chemical Physics*, 1965, **43**, 1480–1489.
6 P. J. Chantry, *Phys. Rev.*, 1968, **172**, 125–136.
7 G. Denifl, D. Muigg, A. Stamatovic and T. Märk, *Chemical Physics Letters*, 1998, **288**, 105 – 110.
8 A. Stamatovic and G. J. Schulz, *The Journal of Chemical Physics*, 1970, **53**, 2663–2667.
9 R. I. Hall, I. Čadež, C. Schermann and M. Tronc, *Phys. Rev. A*, 1977, **15**, 599–610.
10 G. H. Dunn, *Phys. Rev. Lett.*, 1962, **8**, 62–64.
11 L. A. Morgan and J. Tennyson, *Journal of Physics B: Atomic, Molecular and Optical Physics*, 1993, **26**, 2429.
12 D. W. Chandler and P. L. Houston, *The Journal of Chemical Physics*, 1987, **87**, 1445–1447.
13 A. T. Eppink and D. H. Parker, *Review of Scientific Instruments*, 1997, **68**, 3477–3484.
14 C. R. Gebhardt, T. P. Rakitzis, P. C. Samartzis, V. Ladopoulos and T. N. Kitsopoulos, *Review of Scientific Instruments*, 2001, **72**, 3848–3853.
15 D. Townsend, M. P. Minitti and A. G. Suits, *Review of Scientific Instruments*, 2003, **74**, 2530–2539.
16 M. Ashfold, N. Nahler, A. Orr-Ewing, O. Vieuxmaire, R. Toomes, T. Kitsopoulos, I. Anton-Garcia, D. Chestakov, S.-M. Wu and D. Parker, *Physical Chemistry Chemical Physics*, 2006, **8**, 26 – 53.
17 D. Nandi, V. S. Prabhudesai, E. Krishnakumar and A. Chatterjee, *Review of Scientific Instruments*, 2005, **76**, 053107.
18 H. Adaniya, D. S. Slaughter, T. Osipov, T. Weber and A. Belkacem, *Review of Scientific Instruments*, 2012, **83**, 023106.
19 A. Moradmand, J. B. Williams, A. L. Landers and M. Fogle, *Review of Scientific Instruments*, 2013, **84**, 033104.
20 B. Wu, L. Xia, H.-K. Li, X.-J. Zeng and S. Xi Tian, *Review of Scientific Instruments*, 2012, **83**, 013108.
21 E. Wang, X. Shan, Y. Shi, Y. Tang and X. Chen, *Review of Scientific Instruments*, 2013, **84**, 123110.
22 S. X. Tian, B. Wu, L. Xia, Y.-F. Wang, H.-K. Li, X.-J. Zeng, Y. Luo and J. Yang, *Phys. Rev. A*, 2013, **88**, 012708.
23 O. Jagutzki, A. Cerezo, A. Czasch, R. Dorner, M. Hattas, M. Huang, V. Mergel, U. Spillmann, K. Ullmann-Pfleger, T. Weber, H. Schmidt-Bocking and G. Smith, *Nuclear Science, IEEE Transactions on*, 2002, **49**, 2477–2483.
24 D. Nandi and E. Krishnakumar, *International Journal of Mass Spectrometry*, 2010, **289**, 39 – 46.
25 D. S. Slaughter, H. Adaniya, T. N. Rescigno, D. J. Haxton, A. E. Orel, C. W. McCurdy and A. Belkacem, *Journal of Physics B: Atomic, Molecular and Optical Physics*, 2011, **44**, 205203.
26 D. Nandi, V. S. Prabhudesai, B. M. Nestmann and E. Krishnakumar, *Phys. Chem. Chem. Phys.*, 2011, **13**, 1542–1551.
27 K. P. Huber and G. Herzberg, *Molecular Spectra and Molecular Structure IV. Constants of Diatomic Molecules*, Van Nostrand Reinhold Company, New York, (1979).
28 L. M. Branscomb, D. S. Burch, S. J. Smith and S. Geltman, *Phys. Rev.*, 1958, **111**, 504–513.
29 *NIST Chemistry WebBook*, http://webbook.nist.gov/chemistry/.
30 T. F. O'Malley and H. S. Taylor, *Phys. Rev.*, 1968, **176**, 207–221.
31 L. Sanche and G. J. Schulz, *Phys. Rev. Lett.*, 1971, **26**, 943–946.
32 J. Comer and F. H. Read, *Journal of Physics B: Atomic and Molecular Physics*, 1971, **4**, 1678.
33 B. G. Wicke, R. W. Field and W. Klemperer, *The Journal of Chemical Physics*, 1972, **56**, 5758–5770.

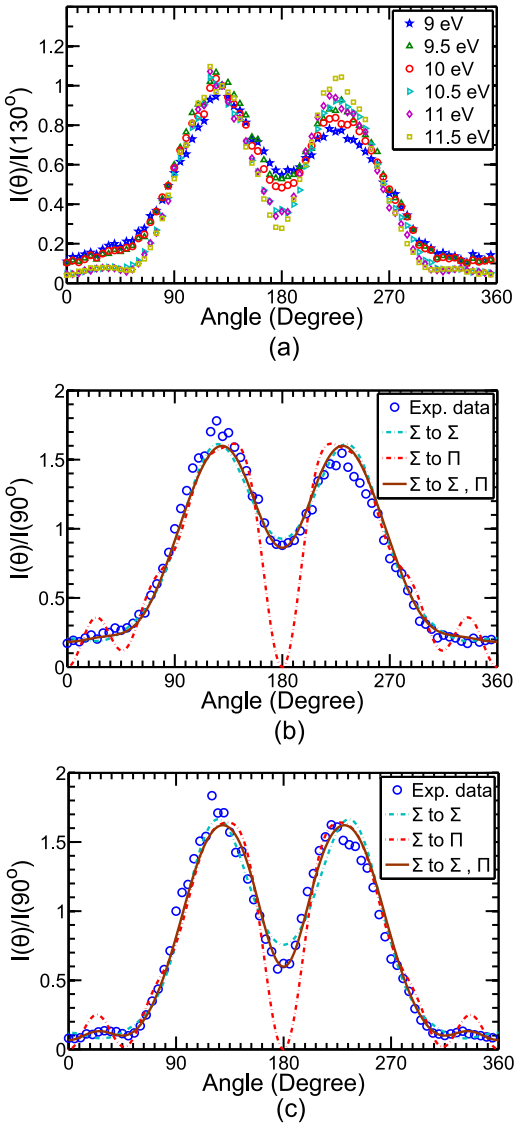

Fig. 5 Angular distribution of the O^- ions created due to process I. (a) Shows the angular distribution for all the six electron energies. (b) The angular distribution at 9.5 eV electron energy fitted with a $\Sigma \rightarrow \Sigma$, $\Sigma \rightarrow \Pi$ single state transition models and Σ to Σ and Π two state model are shown. (c) The angular distribution for 11 eV electron energy with the fitted curve for the same three models.

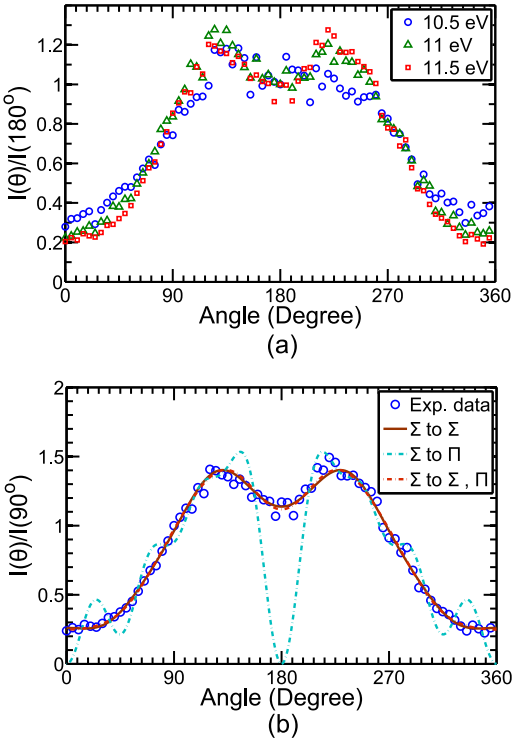

Fig. 6 (a) Angular distribution of the O^- ions created due to process II (b) The angular distribution of the ions for 11.5 eV electron energy fitted with a $\Sigma \rightarrow \Sigma$, $\Sigma \rightarrow \Pi$ single state transition models and Σ to Σ and Π two state model.